Original Research

Dynamic analysis of a needle insertion for soft materials: arbitrary Lagrangian-Eulerian-based three-dimensional finite element analysis

Satoshi Yamaguchi[1*], Kihei Tsutsui[2], Koji Satake[3], Shigehiro Morikawa[4], Yoshiaki Shirai[3], Hiromi T. Tanaka[3]

[1]*Department of Biomaterials Science, Osaka University Graduate School of Dentistry, 1-8 Yamadaoka, Suita, Osaka 565-0871, Japan,*

[2]*Lancemore, Co., M&M2 Building 3F, 5-41-3 Kamata, Ota-ku, Tokyo 144-0052, Japan,*

[3]*College of Information Science and Engineering, Ritsumeikan University, 1-1-1 Nojihigashi, Kusatsu, Shiga 525-8577, Japan,*

[4]*Biomedical MR Science Center, Shiga University of Medical Science, Seta Tsukinowa-chou, Otsu, Shiga 520-2192, Japan*

*Correspondence should be addressed to Satoshi Yamaguchi

Department of Biomaterials Science, Osaka University

1-8 Yamadaoka Suita, Osaka 565-0871, Japan

Tel/Fax: +81-6-6879-2919

Email: yamagu@dent.osaka-u.ac.jp

Abstract

Background: Our goal was to develop a three-dimensional finite element model that enables dynamic analysis of needle insertion for soft materials. To demonstrate large deformation and fracture, we used the arbitrary Lagrangian-Eulerian (ALE) method for fluid analysis. We performed ALE-based finite element analysis for 3 % agar gel and three types of copper needle with bevel tips.

Methods: To evaluate simulation results, we compared the needle deflection and insertion force with corresponding experimental results acquired with a uniaxial manipulator. We studied the shear stress distribution of agar gel on various time scales.

Results: For 30, 45, and 60 degrees, differences in deflections of each needle between both sets of results were 2.424, 2.981, and 3.737 mm, respectively. For the insertion force, there was no significant difference for mismatching area error (p<0.05) between simulation and experimental results.

Conclusions: Our result have a potential to be stepping stone to develop pre-operative surgical planning to estimate an optimal needle insertion path for MR image-guided microwave coagulation therapy and for analyzing large deformation and fracture in biological tissues.

Keywords: *dynamic analysis, needle insertion, finite element analysis, arbitrary Lagrangian-Eulerian method, MR-guided microwave coagulation therapy*

Introduction

Hepatocellular carcinoma (HCC) is the fifth most common cancer and the second leading cause of cancer deaths in men [1]. Magnetic resonance (MR) image-guided microwave coagulation therapy of liver tumors is minimally invasive and has many advantages for both patients and surgeons compared to open surgery [2]. Surgeons are required to insert a needle tip precisely into a targeted location such as a tumor. However, even for expert surgeons, this is not easy because the needle deflection depends on the shape of the needle tip [3, 4].

Several researchers have developed ways to put tip of a needle into a target tumor precisely not only in MR image-guide microwave coagulation therapy of liver tumors but also a number of percutaneous interventions in anesthesia, biopsy, and brachytherapy. Their works can be categorized as modeling insertion force [3, 5-7], tissue deformation [8, 9], and needle deflection [10, 11]; and developing instruments to guide and steer the needle [8, 12-14]. In the modeling insertion force, Okamura, et al. have proposed a model of needle insertion force for the bovine liver [3]. However, they concluded that a more complete model of forces will require a combination of empirical and analytical modeling, with one approach being finite element analysis (FEA). On the

other hand, by extending FEA, Dimaio et al. have developed an interactive virtual needle insertion simulation based on measured planar tissue deformations and needle insertion forces [15]. In addition, they have also proposed the concept of needle steering and formulated a needle manipulation Jacobian based on numerical needle insertion models that include the amounts of needle deflection and soft tissue deformation [16]. Moreover, Alterovitz, et al. have developed a planning system for sensorless needle insertion to reduce the needle insertion error [9].

However, these results have never been clinically applied for human liver tissues [17]. One reason is complex physical phenomena such as fracture involved in large deformation in biological human tissues. Therefore, both clinicians and patients need new approaches. In this respect, time-dependent dynamic fracture analysis in FEA has a potential to solve this issue but it is especially difficult because mesh elimination techniques are required for representing it. In general, FEA with mesh elimination techniques is known as Lagrangian-based FEA for structural analysis. However, a stable calculation is difficult because the finite element mesh needs to flip the shape or release some nodes when the fracture occurs. Thus, we use an arbitrary Lagrangian-Eulerian (ALE) method for fluid analysis that is also suitable for large deformation and fracture

in the continuum model [18].

In this study, we develop a three-dimensional finite element model that enables dynamic analyses of needle insertion with ALE-based FEA using a soft tissue model and three types of needles with bevel tips. To evaluate simulation results, we compared the amount of deflection during needle insertion and the corresponding force along the needle axis with experimental results acquired with a uniaxial manipulator. In addition, we confirmed the shear stress distribution around the needle in simulation results.

Materials and Methods

Characterization of mechanical properties of agar gel

As a phantom study by assuming the use of MR image-guided microwave coagulation therapy in open-MRI [19-21], we used 3 % agar gel (Agar 010-15815, Wako Pure Chemical Industries, Osaka, Japan) instead of liver tissue as an isotropic and nonlinear elastic material [8]. To acquire a nominal stress and nominal strain curve of the agar gel, we performed a uniaxial compression test and three-points bending test using a compact tabletop universal tester (EZ Test, Shimadzu, Kyoto, Japan). In general, the nominal stress and nominal strain curve is generated from results of the uniaxial compression and tension tests. However, for agar gel, it is difficult to perform a tension test because of its wetness. So, as the first step, a bending elastic modulus and a bending strain were calculated by the three-points bending test following ISO 178. Then, a nominal strain combining the nominal strain of the bending test (positive) and the compression test (negative) was used as input data to calculate a nominal stress according to the strain energy function W which is a function of the relative volume, J[22]

$$W^* = \sum_{i=1}^{3} \sum_{j=1}^{n} \frac{\mu_j}{\alpha_j} \left(\lambda_i^{*\alpha_j} - 1 \right) + K\left(J - 1 - \ln J \right) \qquad (1)$$

where the asterisk (*) indicates that the volumetric effects have been eliminated from the principal stretches, λ_j^*. The number of terms, n, may vary from 1 to 8 inclusive, and the bulk modulus is K. The jth shear modulus and exponent are μ_j and α_j, respectively. In this study, we used $n = 3$ as the number of terms. Finally, we manually estimated six parameters until correct nominal stress was obtained by demonstrating displacement-force curve similar to both the compression and three-points bending tests through Lagrangian-based FEA with commercial software (ANSYS LS-DYNA Ver. 971 R6.0 single, Livermore Software Technology, CA, USA), iteratively. We prepared ten test pieces for the test (compression test: 60×20×4 mm, three-points bending test: 60×20×20 mm, cross-head speed: 2 mm/sec). Young's modulus and Poisson's ratio of the copper needle C1100 (Custom-made, Umihira, Kyoto, Japan) used were 117 GPa and 0.33 respectively. The copper is used as one of MR compatible materials [23].

Needle insertion experiment

To evaluate this model, we performed an experiment to measure needle deflection and reaction force with a uniaxial insertion device (Custom-made, Umihira, Kyoto,

Japan) (**Fig. 1**) by 8000 Hz sampling rates. The sizes of the needle and agar were φ1.6 × 150 mm based on MR compatible 14-G puncture needle [2]) and 150 × 40 × 200 mm, respectively. The angles of the bevel needle tip were 30, 45, and 60°. The needle was inserted into the agar gel at constant velocity 2 mm/sec with a penetration depth of 100 mm by assuming an application with open-MRI robot [23]. After insertion, we took photos from the lateral side with a digital camera (IXY Digital 2000IS, Canon, Ota-ku, Japan) to measure the needle deflection with image processing software (Image J, NIH, Bethesda, MD, USA) (n = 5).

ALE-based finite element analysis

We developed ALE-based FEA models as shown in **Fig. 2A**. The model consists of the agar fixed on the lower surface. The displacement 100 mm along the z-axis was applied to the rigid part (Yellow part of **Fig. 2A**) of the needle. The frictional coefficient 0.01 was empirically set as the contact condition between the needle and the agar. The same geometries as the experimental model were adopted for the sizes of the needle and agar, and the angles of the bevel needle tip. Also, the needles have no tubular structure because an outer needle was inserted into liver with an inner coagulation probe as one

needle. We generated the needle mesh using rectangular elements as a shell, and generated the meshes of the agar with hexahedral elements as a solid (**Fig. 2B, 2C**). The number of meshes totaled 297,014 elements. The size of the smallest mesh was 0.375 mm in all models. We performed standard ALE-based FEA including ANSYS LS-DYNA. Material models of the needle and the agar gel applied linear elastic material (MAT_001) and isotropic elastic-plastic material (MAT_124) applying a nominal stress and nominal strain curve estimated via the above procedure, respectively.

Statistical analysis

We statistically compared between the simulation and experimental results of acquired force and displacement curve using a two-factor ANOVA ($p<0.05$). An average curve was generated among experimental results for each bevel angle. We calculated the mismatching area by subtracting a domain bounded by the acquired force and displacement curve of simulation results from that of experimental results.

Results

Mechanical properties of agar gel

Fig. 3 shows mechanical properties of the agar gel. A nominal stress and nominal strain curve shows different trends for compression and tension.

Needle deflection

A comparison of needle deflections between the experimental and simulation results were shown in **Fig. 4**. For 30, 45, and 60 degrees, differences in mean deflections of each needle between both sets of results were 2.424, 2.981, and 3.737 mm, respectively. **Fig. 5** shows photos from the vertical direction for lateral side of the 30-degree needle at 0, 20, 40, 60, 80, and 100 mm, respectively.

Needle insertion force

A comparison of needle insertion forces was shown in **Fig. 6**. For experimental and simulation results, the mismatching areas were 189, 238, and 222; and 246, 294, and 317, respectively (**Fig. 7**). The needle reaction forces showed no significant difference between simulation and experimental results (p>0.05). In addition, the

post-puncture force gradually increased in all cases.

Shear stress distribution

The shear stress distribution in a cross-sectional surface along the x-z plane from steps 0 to 100 for every 20th step for 30 degree was shown in **Fig. 8**. Shear stresses in each model had different distributions affecting the needle tip shape (**S1**, **S2**, **and S3**). For 30, 45, and 60 degrees, the maximum shear stresses in last step were 0.0267, 0.0347, and 0.0350 MPa, respectively. The maximum shear stress appeared near the needle tip for all time scales and all cases.

Discussion

In this study, we developed a three-dimensional finite element model for dynamic fracture analysis of needle insertion through ALE-based FEA using an acquired nominal stress and nominal strain curve of agar gel. Applying an ALE method to fluid analysis makes it possible to do structure analysis with large deformation and fracture. Our results help to predict the needle deflection, insertion force, and shear stress distributions during needle insertion as pre-operative surgical planning *in silico*. In addition, it can help design new shapes of clinical needles to reduce the burden on patients.

For the nominal stress and nominal strain curve, it is clear that the agar gel has different compression and tension properties. Thus, in this study, we used an isotropic elastic-plastic material (MAT_124 that is the material number in ANSYS/LS-DYNA). For the different compression and tension properties, one should apply Ogden (MAT_77O) or Mooney-Rivlin (MAT_27) material, which can exhibit hyper-elastic rubber properties [24]. However, both hyper-elastic rubber models in ANSYS/LS-DYNA were supported for only low strain range. Thus, by following the Ogden equations (1), the nominal stress and nominal strain were estimated and applied

into MAT_124 that can use a different stress/strain curve for compression and tension.

While the differences of needle deflection were 2.42, 2.98, and 3.73 mm, respectively (**Fig. 4**), the size of a typical target tumor is about 30 mm [25-27]. These results suggest that our simulation results are in the allowable range for clinical applications such as pre-operative surgical planning. However, these error rates of the mismatching errors for 30, 45, and 60 degrees were 23, 19, and 30 %, respectively and these results seem inaccurate even given the allowable range for clinical applications. One of reasons is the material property of the agar gel that can vary time-dependently in terms of the room temperature. Also, the agar gel has difficult to generate it as a complete isotropic material. As one of solutions, we are investigating generation of samples using a magnetic stirrer. In addition, our simulations used a great deal of time, about 70 hours to finish analysis. At this time, we can say with fair certainty that real-time simulation of intra-operative surgical navigation or virtual reality training to train hand skill is difficult; the research may be useful for pre-operative surgical planning instead. As one solution for this issue, the general purpose graphics processing unit (GPGPU) [28] has been developed and has accelerated the use of various commercial software in recent years. In other words, real-time ALE-based FEA will

appear soon.

For the insertion force (**Fig. 6**), there was no peak during needle puncture compared to a result obtained by Okamura et al [3]. It is for this reason that we eliminate the thin membrane on top of the surface of agar gel before the experiment and have absolutely no membrane in the finite element model. Actually, in MR image-guided microwave coagulation therapy, an incision line by surgical instruments is marked out on abdominal skin to reduce renitences of the needle insertion. In both simulation and experimental results, the increase of insertion force in post-puncture is due to the influence of friction between the agar gel and the needle. Also, the oscillation of the curve (**Fig. 6**) caused a stick-slip effect due to friction [3, 15, 29, 30].

Finally, shear stress in the agar gel is distributed along the needle and seems generally undulating. This reason is, as mentioned above, also due to the influence of the stick-slip effect. In addition, one of the reasons for gradually rising of maximum shear stress is that the shape of the needle tip becomes increasingly similar to a cylindrical solid as the bevel angle increases. In this study, a maximum shear stress was adopted to confirm the stress distributions because the maximum shear stress is located as a safe side in comparison with the maximum principal stress and maximum strain

energy.

For more clinical situation, the estimation of stress and strain curve of bovine liver tissue as isotropic and nonlinear elastic material [8] and ALE-based FEA are ongoing to investigate availability of our approach. Within the limitations of finite element study, these solutions may become a strong tool for understanding the mechanisms of various complex biological phenomena such as mosquito needle insertion into human skin [31-33] and cell injection [34, 35].

Conclusion

In this study, we developed a three-dimensional finite element model that enables dynamic analysis of needle insertion by applying the ALE-based three-dimensional FEA. Our result have a potential to be stepping stone to develop pre-operative surgical planning to estimate an optimal needle insertion path for MR image-guided microwave coagulation therapy and for analyzing large deformation and fracture in biological tissues.

Acknowledgments

This study was supported by Grants-in-Aid for Scientific Research Nos. 24592955 and 21240017 from the Japan Society for the Promotion of Science, Japan.

Author Contributions

Conceived and designed the experiments: SY, KT, KS, SM. Performed the experiments: SY, KS. Performed the simulations: SY, KT. Analyzed the data: SY. Contributed reagents/materials/analysis tools: SY, KS, SM, YS. Wrote the paper: SY. Administrative support: YS, HT.

References

[1] Wong VW, Chan HL, Prevention of hepatocellular carcinoma: a concise review of contemporary issues. *Ann Hepatol* 11 (2011) 284-293.

[2] Morikawa S, Naka S, Murakami K, Kurumi Y, Shiomi H, Tani T, Haque HA, Tokuda J, Hata N, Inubushi T, Preliminary clinical experiences of a motorized manipulator for magnetic resonance image-guided microwave coagulation therapy of liver tumors. *Am J Surg* 198 (2009) 340-347.

[3] Okamura AM, Simone C, O'Leary MD, Force modeling for needle insertion into soft tissue. *IEEE Trans Biomed Eng* 51 (2004) 1707-1716.

[4] Abolhassani N, Patel R, Moallem M, Needle insertion into soft tissue: A survey. *Med Eng Phys* 29 (2007) 413-431.

[5] Podder TK, Sherman J, Messing EM, Rubens DJ, Fuller D, Strang JG, Brasacchio RA, Yu Y, Needle insertion force estimation model using procedure-specific and patient-specific criteria. *Conf Proc IEEE Eng Med Biol Soc* 1 (2006) 555-558.

[6] Kobayashi Y, Sato T, Fujie MG, Modeling of friction force based on

relative velocity between liver tissue and needle for needle insertion simulation. *Conf Proc IEEE Eng Med Biol Soc 2009* (2009) 5274-5278.

[7] Asadian A, Kermani MR, Patel RV, A Novel Force Modeling Scheme for Needle Insertion Using Multiple Kalman Filters. *IEEE Trans Instrum Meas* 61 (2012) 429-438.

[8] Kobayashi Y, Onishi A, Watanabe H, Hoshi T, Kawamura K, Hashizume M, Fujie MG, Development of an integrated needle insertion system with image guidance and deformation simulation. *Comput Med Imaging Graph* 34 (2010) 9-18.

[9] Alterovitz R, Goldberg KY, Pouliot J, Hsu IC, Sensorless motion planning for medical needle insertion in deformable tissues. *IEEE Trans Inf Technol Biomed* 13 (2009) 217-225.

[10] Park YL, Elayaperumal S, Daniel B, Ryu SC, Shin M, Savall J, Black RJ, Moslehi B, Cutkosky MR, Real-Time Estimation of 3-D Needle Shape and Deflection for MRI-Guided Interventions. *IEEE/ASME Trans Mechatron* 15 (2010) 906-915.

[11] Baegert C, Villard C, Schreck P, Soler L, Gangi A, Trajectory

optimization for the planning of percutaneous radiofrequency ablation of hepatic tumors. *Comput Aided Surg* 12 (2007) 82-90.

[12] Misra S, Reed KB, Schafer BW, Ramesh KT, Okamura AM, Mechanics of flexible needles robotically steered through soft tissue. *Int J Rob Res* 29 (2010) 1640-1660.

[13] Wood NA, Shahrour K, Ost MC, Riviere CN, Needle steering system using duty-cycled rotation for percutaneous kidney access. *Conf Proc IEEE Eng Med Biol Soc 2010* (2010) 5432-5435.

[14] Asadian A, Kermani MR, Patel RV, Robot-assisted needle steering using a control theoretic approach. *J Intell Robot Syst* 62 (2011) 397-418.

[15] DiMaio SP, Salcudean SE, Interactive simulation of needle insertion models. *IEEE Trans Biomed Eng* 52 (2005) 1167-1179.

[16] DiMaio SP, Salcudean SE, Needle steering and motion planning in soft tissues. *IEEE Trans Biomed Eng* 52 (2005) 965-974.

[17] Majewicz A, Marra S, van Vledder M, Lin M, Choti M, Song D, Okamura A, Behavior of tip-steerable needles in ex vivo and in vivo tissue. *IEEE Trans Biomed Eng* 59 (2012) 2705-2715.

[18] Hirt CW, Amsden AA, Cook JL, An arbitrary Lagrangian-Eulerian computing method for all flow speeds. *J Comput Phys* 14 (1974) 227-253.

[19] Demura K, Morikawa S, Murakami K, Sato K, Shiomi H, Naka S, Kurumi Y, Inubushi T, Tani T, An easy-to-use microwave hyperthermia system combined with spatially resolved MR temperature maps: phantom and animal studies. *J Surg Res* 135 (2006) 179-186.

[20] Keserci BM, Kokuryo D, Suzuki K, Kumamoto E, Okada A, Khankan AA, Kuroda K, Near-real-time feedback control system for liver thermal ablations based on self-referenced temperature imaging. *Eur J Radiol* 59 (2006) 175-182.

[21] Tokuda J, Morikawa S, Haque HA, Tsukamoto T, Matsumiya K, Liao H, Masamune K, Dohi T. Adaptive 4D MR imaging using navigator-based respiratory signal for MRI-guided thrapy. *Magn Reson Med* 59 (2008) 1051-1061.

[22] Ogden RW, Non-linear elastic deformations. Canada: General Publishing Company, Ltd.; 1984.

[23] Hata N, Tokuda J, Hurwitz S, Morikawa S, MRI-compatible

manipulator with remote-center-of-motion control. *J Magn Reson Imaging* 27 (2008) 1130-1138.

[24] Martínez-Martínez F, Lago MA, Rupérez MJ, Monserrat C, Analysis of several biomechanical models for the simulation of lamb liver behaviour using similarity coefficients from medical image. *Comput Methods Biomech Biomed Engin* 16 (2013) 747-757.

[25] Hur H, Ko YT, Min BS, Kim KS, Choi JS, Sohn SK, Cho CH, Ko HK, Lee JT, Kim NK, Comparative study of resection and radiofrequency ablation in the treatment of solitary colorectal liver metastases. *Am J Surg* 197 (2009) 728-736.

[26] Kudo M, Okanoue T, Panel CPMHE, Management of hepatocellular carcinoma in Japan: Consensus-based clinical practice manual proposed by the Japan Society of Hepatology. *Oncology* 72 (2007) 2-15.

[27] Makuuchi M, Kokudo N, Arii S, Futagawa S, Kaneko S, Kawasaki S, Matsuyama Y, Okazaki M, Okita K, Omata M, Saida Y, Takayama T, Yamaoka Y, Development of evidence-based clinical guidelines for the diagnosis and treatment of hepatocellular carcinoma in Japan. *Hepatol Res*

38 (2008) 37-51.

[28] Dick C, Georgii J, Westermann R, A real-time multigrid finite hexahedra method for elasticity simulation using CUDA. *Simul Model Pract Th* 19 (2011) 801-816.

[29] Chentanez N, Alterovitz R, Ritchie D, Cho L, Hauser KK, Goldberg K, Shewchuk JR, O'Brien JF, Interactive simulation of surgical needle insertion and steering. *ACM Trans Graphic* 88 (2009) 1-10.

[30] Nienhuys HW, van der Stappen AF, editors. A computational technique for interactive needle insertions in 3D nonlinear material. Robotics and Automation, *Conf Proc IEEE Robot Automat* 2 (2004) 2061-2067.

[31] Izumi H, Yajima T, Aoyagi S, Tagawa N, Arai Y, Hirata M, Combined harpoonlike jagged microneedles imitating mosquito's proboscis and its insertion experiment with vibration. *IEEJ Trans Electrical Electron Eng* 3 (2008) 425-431.

[32] Ramasubramanian MK, Barham OM, Swaminathan V, Mechanics of a mosquito bite with applications to microneedle design. *Bioinspir Biomim*

3 (2008) 046001.

[33] Aoyagi S, Izumi H, Fukuda M, Biodegradable polymer needle with various tip angles and consideration on insertion mechanism of mosquito's proboscis. *Sensor Actuat A-Phy* 143 (2008) 20-28.

[34] Tan YH, Sun D, Huang WH, Cheng SH, Characterizing mechanical properties of biological cells by microinjection. *IEEE Trans Nanobiosci* 9 (2010) 171-180.

[35] Berry MF, Engler AJ, Woo YJ, Pirolli TJ, Bish LT, Jayasankar V, Morine KJ, Gardner TJ, Discher DE, Sweeney HL, Mesenchymal stem cell injection after myocardial infarction improves myocardial compliance. *Am J Physiol Heart Circ Physiol* 290 (2006) H2196-2203.

Summary

Hepatocellular carcinoma (HCC) is the fifth most common cancer and the second leading cause of cancer deaths in men. Radiofrequency ablation (RFA) therapy of liver tumors is minimally invasive and has many advantages for patients such as minimal pain and scarring and quick recovery compared to open surgery. Surgeons are required to insert a needle tip precisely into a targeted location such as a tumor. However, even for expert surgeons, this is not easy because the needle deflection depends on the shape of the needle tip.

Our goal was to develop a three-dimensional finite element model that enables dynamic analysis of needle insertion for soft materials. To demonstrate large deformation and fracture, we used the arbitrary Lagrangian-Eulerian (ALE) method for fluid analysis. We performed ALE-based finite element analysis for 3 % agar gel and three types of copper needle with bevel tips by assuming to apply MR image-guided microwave coagulation therapy in Open-MRI.

To evaluate simulation results, we compared the amount of deflection during needle insertion and the corresponding force along the needle axis with experimental results acquired with a uniaxial manipulator. In addition, we confirmed the shear stress

distribution around the needle in simulation results.

For 30, 45, and 60 degrees, differences in deflections of each needle between both sets of results were 2.424, 2.981, and 3.737 mm, respectively. For the insertion force, there was no significant difference for mismatching area error ($p<0.05$) between simulation and experimental results.

In this study, we developed three-dimensional finite element model that enables dynamic analysis of needle insertion by applying the ALE-based three-dimensional FEA. Our result shows that it is useful for pre-operative surgical planning for liver cancer surgery by radiofrequency ablation therapy and for analyzing large deformation and fracture in biological tissues. For the future, ALE-based FEA will become widely used to explain fracture mechanisms in biological tissues.

Figure

Figure 1

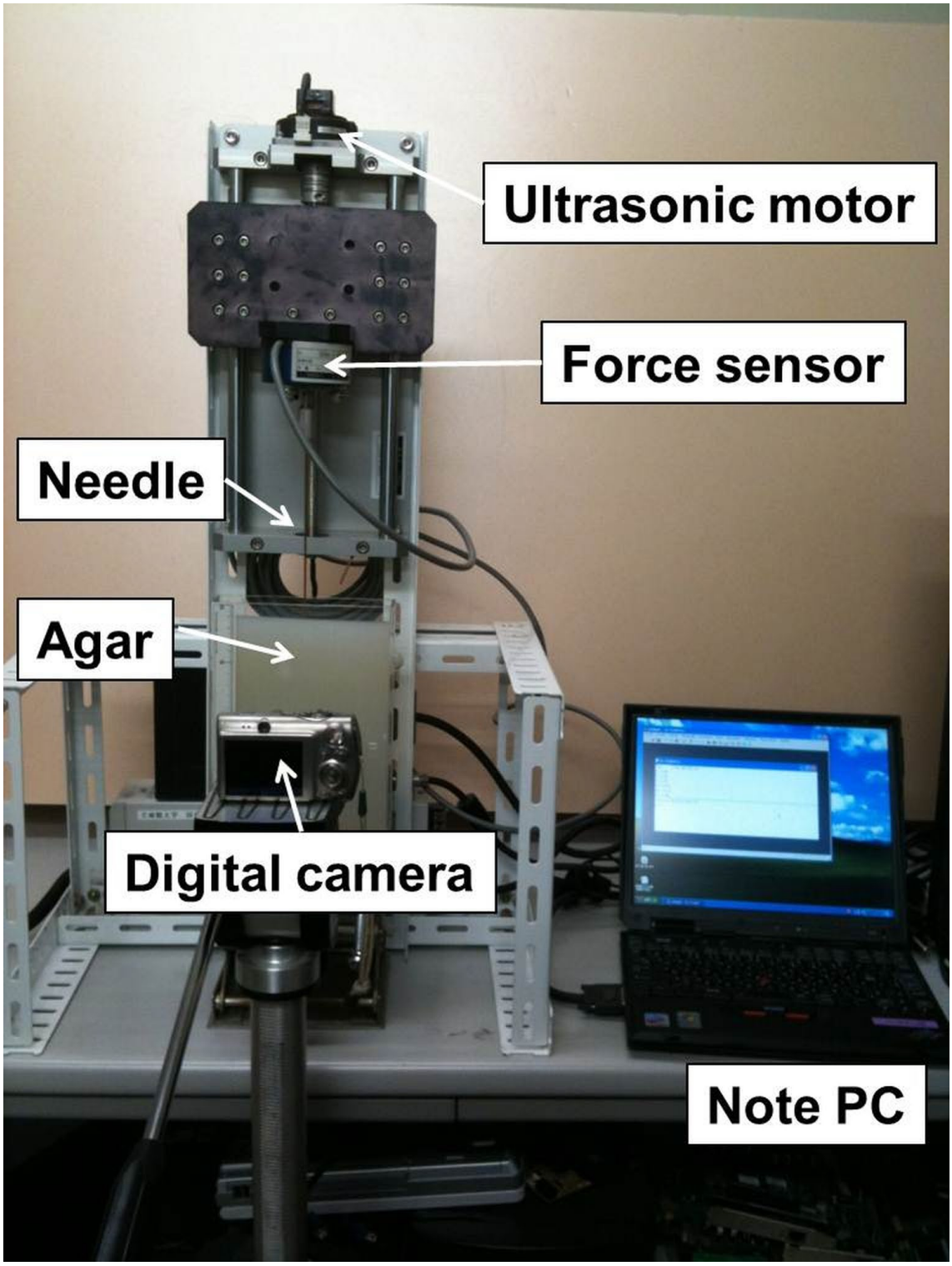

Figure 2

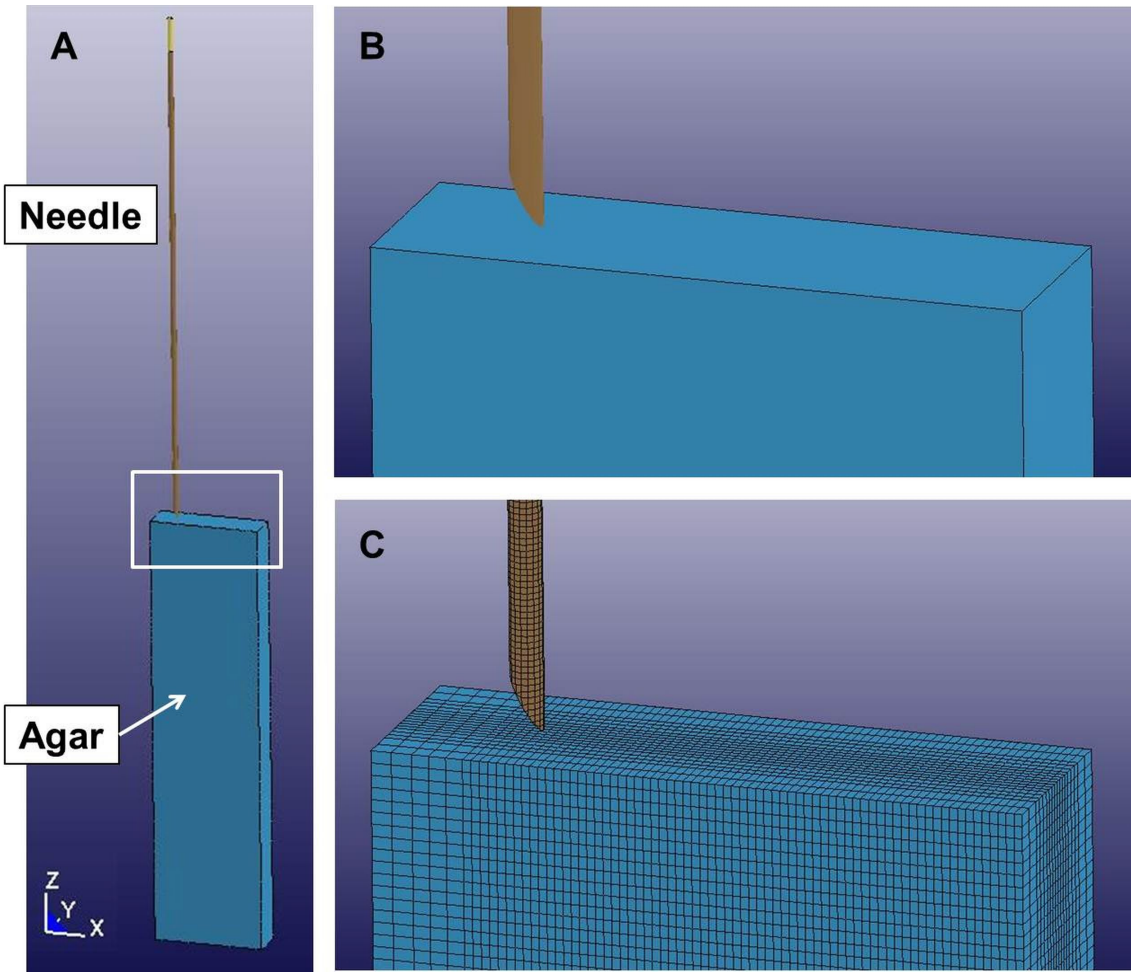

Figure 3

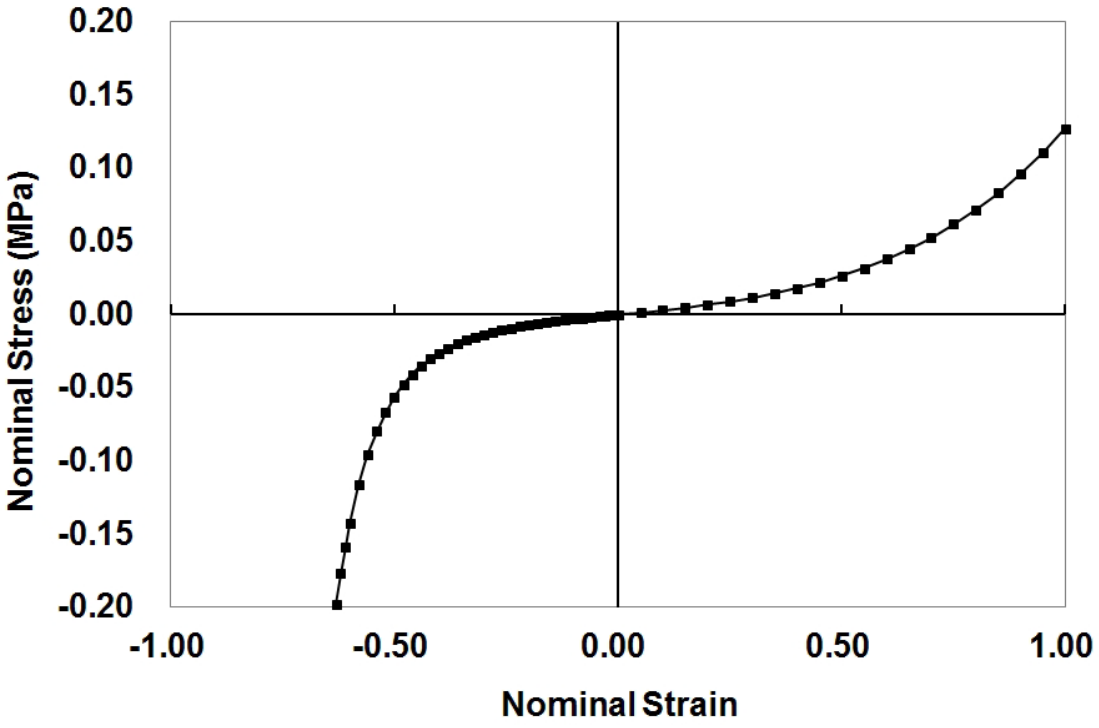
0.20
0.15
0.10
0.05
0.00
-0.05
-0.10
-0.15
-0.20
Nominal Stress (MPa)
-1.00
-0.50
0.00
0.50
1.00
Nominal Strain

Figure 4

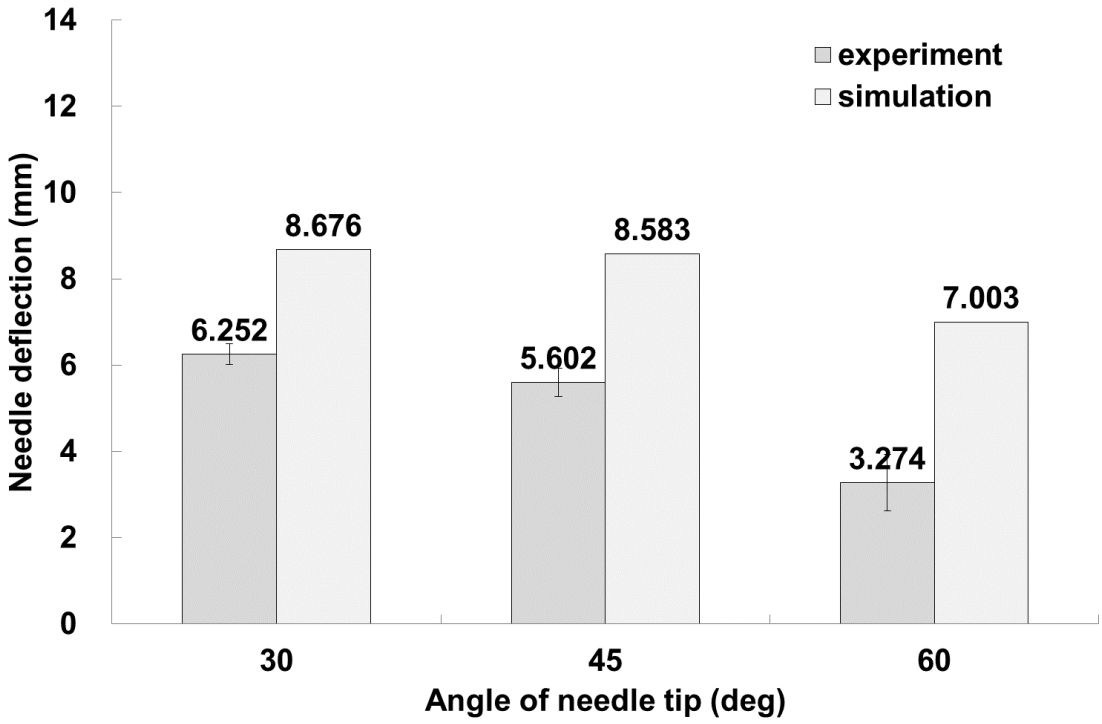
14
12
10
8
6
4
2
0
Needle deflection (mm)
experiment
simulation
8.676
8.583
7.003
6.252
5.602
3.274
30
45
60
Angle of needle tip (deg)

Figure 5

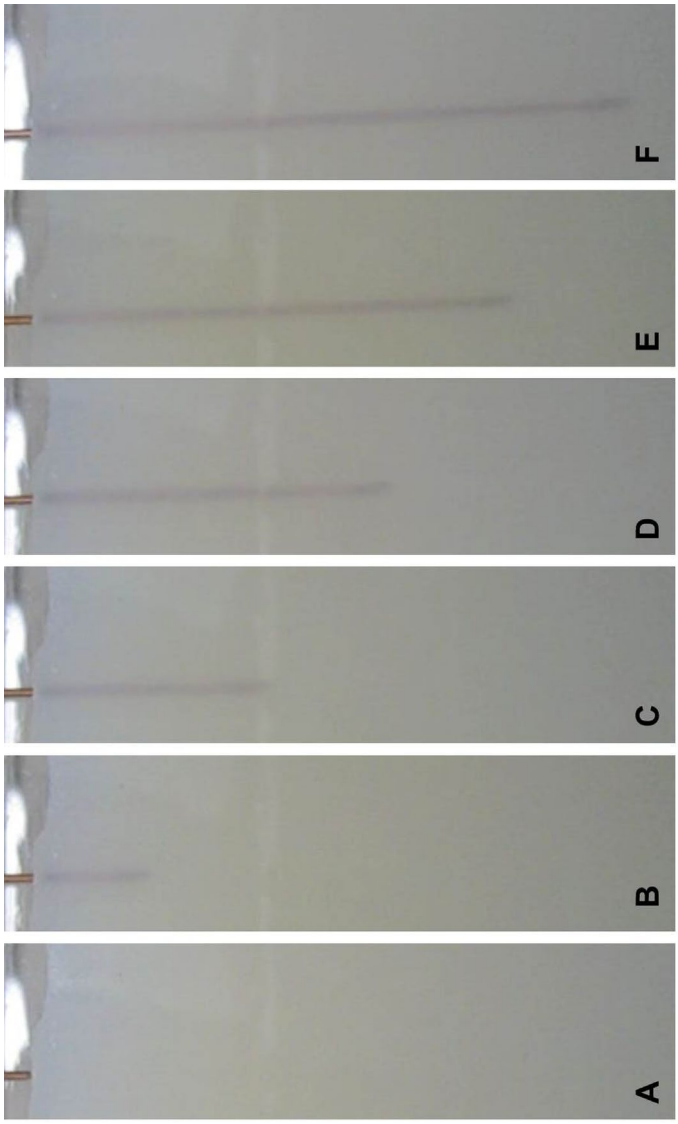

Figure 6

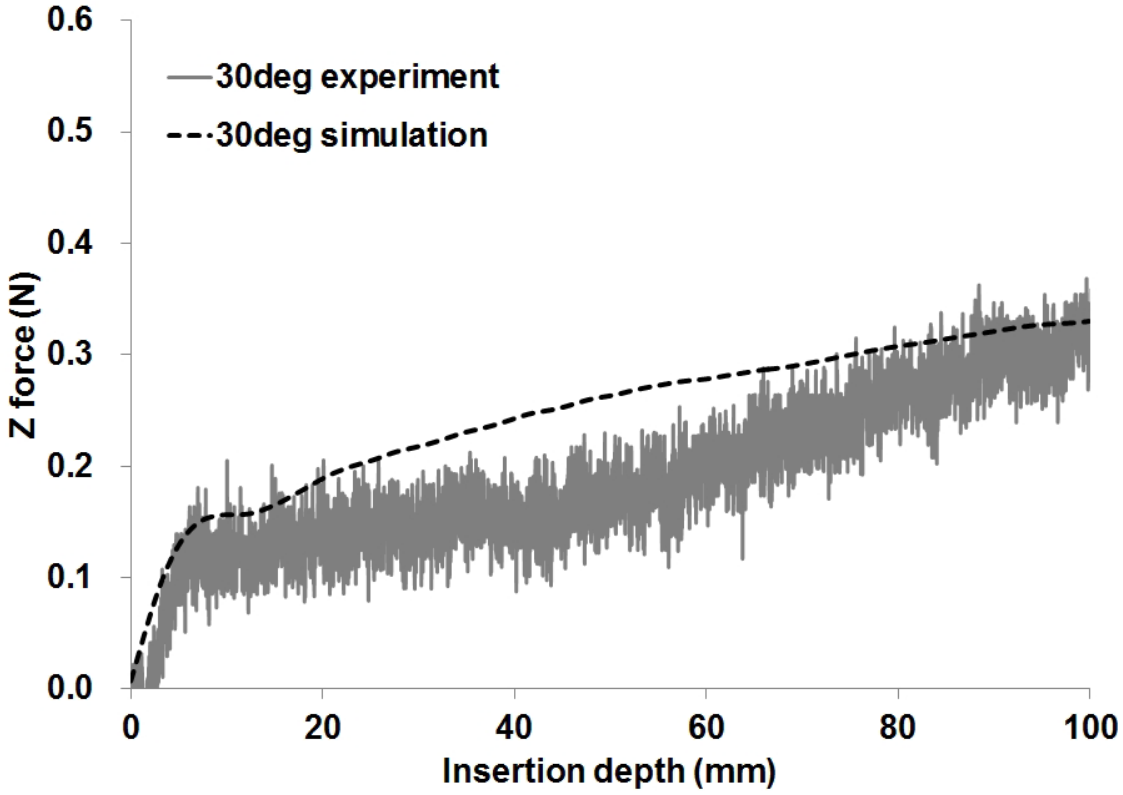
0.6
0.5
0.4
0.3
0.2
0.1
0.0
Z force (N)
30deg experiment
30deg simulation
0
20
40
60
80
100
Insertion depth (mm)

Figure 7

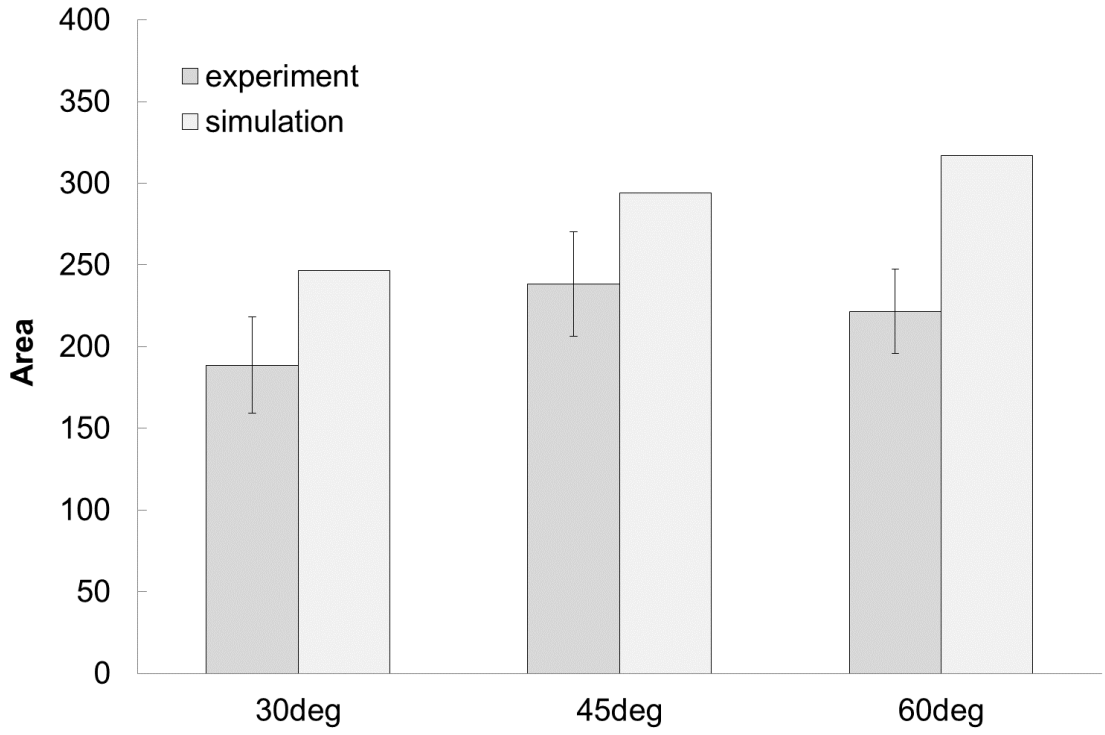
400
350
300
250
200
150
100
50
0
Area
experiment
simulation
30deg
45deg
60deg

Figure 8

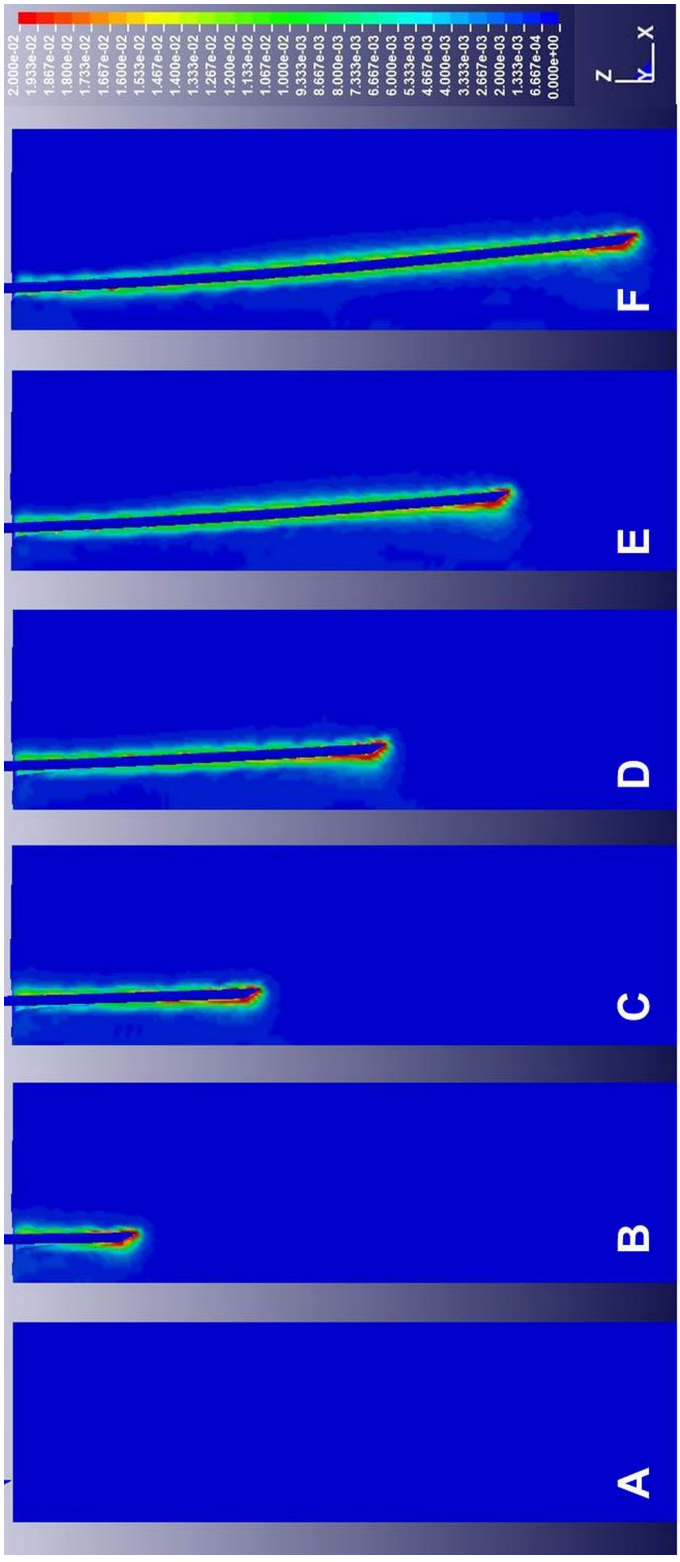
2.000e-02
1.933e-02
1.867e-02
1.800e-02
1.733e-02
1.667e-02
1.600e-02
1.533e-02
1.467e-02
1.400e-02
1.333e-02
1.267e-02
1.200e-02
1.133e-02
1.067e-02
1.000e-02
9.333e-03
8.667e-03
8.000e-03
7.333e-03
6.667e-03
6.000e-03
5.333e-03
4.667e-03
4.000e-03
3.333e-03
2.667e-03
2.000e-03
1.333e-03
6.667e-04
0.000e+00
Z
X
A
B
C
D
E
F

Figures legends

Figure 1. Uniaxial manipulator.

Figure 2. Finite element model for needle insertion analysis. (A) Whole image (B) Solid model (C) Meshed model.

Figure 3. Nominal stress and nominal strain curve of agar gel.

Figure 4. Comparison of needle deflection at 100mm in depth between results of experiment and simulation.

Figure 5. Needle deflection (30 deg). (A) 0mm, (B) 20mm, (C) 40mm, (D) 60mm, (E) 80mm, (F) 100mm.

Figure 6. Comparison of reaction force between results of experiment and simulation.

Figure 7. Comparison of mismatching area between results of experiment and simulation.

Figure 8. Shear stress distributions (30 deg). (A) step 0, (B) step 20, (C) step 40, (D) step 60, (E) step 80, (F) step 100.

S1. Shear stress distributions for 30 deg.

S2. Shear stress distributions for 45 deg.

S3. Shear stress distributions for 60 deg.

Highlights

1. We performed ALE-based finite element analysis for agar gel and copper needles.

2. We compared simulation results with corresponding experimental results.

3. Deflections of each needle between both sets of results were different.

4. There was no significant difference for mismatching area error.

5. Our results have a potential to use as pre-operative surgical planning.